Membrane Orientation and Lateral Diffusion of BODIPY-Cholesterol as a Function of Probe Structure

Lukasz M. Solanko,[†] Alf Honigmann,[¶] Henrik Skov Midtiby,[‡§] Frederik W. Lund,[†] Jonathan R. Brewer,[†‡] Vjekoslav Dekaris,[‖] Robert Bittman,[‖] Christian Eggeling,[¶**] and Daniel Wüstner[†*]

[†]Department of Biochemistry and Molecular Biology, [‡]MEMPHYS Center for Biomembrane Physics, Department of Pharmacy, Chemistry and Physics, and [§]Institute for Chemical, Biological and Environmental Technology, University of Southern Denmark, Odense M, Denmark; [¶]Max Planck Institute for Biophysical Chemistry, Department of NanoBiophotonics, Am Fassberg 11, Göttingen, Germany; [‖]Department of Chemistry and Biochemistry, Queens College, The City University of New York, Flushing, New York; and **Human Immunology Unit, Weatherall Institute of Molecular Medicine, University of Oxford, Oxford, United Kingdom

ABSTRACT Cholesterol tagged with the BODIPY fluorophore via the central difluoroboron moiety of the dye (B-Chol) is a promising probe for studying intracellular cholesterol dynamics. We synthesized a new BODIPY-cholesterol probe (B-P-Chol) with the fluorophore attached via one of its pyrrole rings to carbon-24 of cholesterol (B-P-Chol). Using two-photon fluorescence polarimetry in giant unilamellar vesicles and in the plasma membrane (PM) of living intact and actin-disrupted cells, we show that the BODIPY-groups in B-Chol and B-P-Chol are oriented perpendicular and almost parallel to the bilayer normal, respectively. B-Chol is in all three membrane systems much stronger oriented than B-P-Chol. Interestingly, we found that the lateral diffusion in the PM was two times slower for B-Chol than for B-P-Chol, although we found no difference in lateral diffusion in model membranes. Stimulated emission depletion microscopy, performed for the first time, to our knowledge, with fluorescent sterols, revealed that the difference in lateral diffusion of the BODIPY-cholesterol probes was not caused by anomalous subdiffusion, because diffusion of both analogs in the PM was free but not hindered. Our combined measurements show that the position and orientation of the BODIPY moiety in cholesterol analogs have a severe influence on lateral diffusion specifically in the PM of living cells.

INTRODUCTION

Understanding the lateral organization of cholesterol in the plasma membrane (PM) is of major importance for development of new models of cell membrane structure and organization (1). One prominent model assumes lipid-based domain architecture in so-called rafts stabilized by specific sphingolipid-cholesterol interactions. In its original form, that model proposed lateral enrichment of cholesterol in ordered domains in the PM (2). Attempts to visualize sterol domains in the PM using the intrinsically fluorescent close cholesterol mimics cholestatrienol (CTL) and dehydroergosterol (DHE), however, were unsuccessful, and apparent enrichment was found to be a direct consequence of the high submicroscopic curvature of the cell surface (3,4). Characterization of membrane heterogeneity has been performed by several biophysical methods and agreement exists that eventual formation of nanoclusters depends on cholesterol and the cytoskeleton (5–7). How cholesterol itself moves in the PM, however, remains enigmatic. Although intrinsically fluorescent sterols are theoretically the probes of choice to answer this question, the unfavorable photophysical properties of DHE and CTL, which include ultraviolet absorption and ultraviolet fluorescence, low quantum yield, and high photobleaching propensity, make measurement of sterol dynamics within membranes using these cholesterol analogs very challenging. Most cholesterol analogs with an extrinsic fluorophore, however, such as cholesterol tagged with nitrobenzoxadiazole (NBD) fail to behave like cholesterol in model and cell membranes (8,9). Bodipy-cholesterol (B-Chol) (Fig. 1 *A*) is a recently designed cholesterol analog with similar, although not identical, properties to cholesterol and CTL or DHE (10–12). B-Chol partitions into the liquid ordered (l_o) phase in ternary model membranes, although with lower affinity than DHE (12–15). It is transported from the PM to recycling endosomes with similar kinetics and ATP-dependence as DHE, but shows some miss-targeting to lipid droplets in cells with high fat content (12,16). Recently, we demonstrated the potential of B-Chol for tracking vesicular sterol transport with high accuracy, allowing for comparison with diffusion models and for determination of the impact of the cytoskeleton on sterol trafficking (17).

It is well known that cholesterol increases the ordering of phospholipid acyl chains and thereby increases the lateral packing of lipids in the bilayer (18). This property of cholesterol is central for its function in regulating membrane fluidity, bending rigidity, and permeability. The tilt, i.e., the rotation of cholesterol's long molecular axis relative to the bilayer normal has been proposed to be a main determinant of the ability of this sterol to order phospholipid acyl chains and condense lipid bilayers (19). NMR and fluorescence spectroscopy in concert with neutron scattering experiments showed that, despite its strong average orientation, cholesterol undergoes anisotropic motion in the bilayer; fast rotation in discrete jumps is paralleled by rapid out-of-plane diffusion parallel to the membrane normal, both with GHz frequency (20,21). Attachment of fluorophores to cholesterol

Submitted June 26, 2013, and accepted for publication September 16, 2013.

*Correspondence: wuestner@bmb.sdu.dk

Editor: Tobias Baumgart.

0006-3495/13/11/2082/11 $2.00

http://dx.doi.org/10.1016/j.bpj.2013.09.031

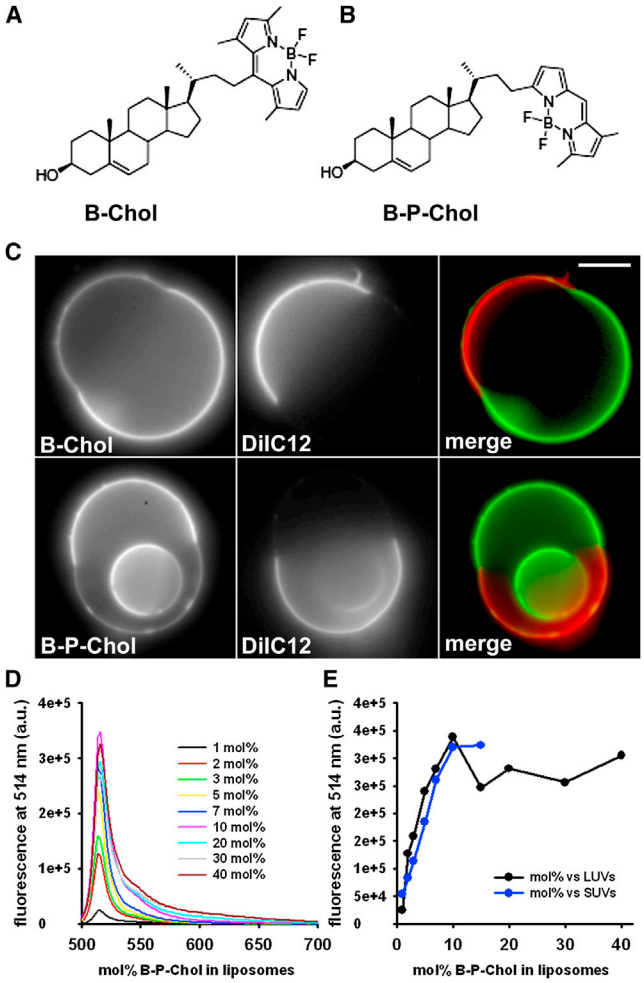

FIGURE 1 Structure, domain partitioning, and self-quenching of BODIPY-cholesterol probes. (*A* and *B*) Structure of B-Chol (*A*) and B-P-Chol (*B*). (*C*) Partitioning of B-Chol (*upper row*) and B-P-Chol in GUVs with l_o/l_d phase coexistence. GUVs were prepared from DPPC, DOPC, and cholesterol in mol percentages of 33:33:33 together with 0.5 mol % of DiIC12 and either B-Chol or B-P-Chol (0.5 mol %) and imaged on a wide field microscope as described in the Supporting Material. Both sterol probes enrich in the DiIC12 poor l_o phase (*green in color* merge in the *most right panels*). (*D*) Emission spectra of B-P-Chol in LUVs made of POPC and increasing concentrations of the sterol probe. A characteristic fluorescence peak at 515 nm but no red-shifted side maximum as in other BODIPY-lipids is found. (*E*) The emission peak at 515 nm was plotted as a function of the probe mole fraction in LUVs (*black symbols* and *line*) and SUVs (*blue symbol* and *line*). Scale bar = 10 μm.

is expected to increase the molecular tilt and thereby locally perturb the membrane structure. This has been observed in molecular dynamics (MD) simulations of B-Chol compared to cholesterol (10). Thus, to assess the potential of fluorescent analogs of cholesterol to mimic the properties of endogenous cholesterol requires taking the orientation of the flurophore into account. Here, we report the synthesis and characterization of a new, to our knowledge, BODIPY-cholesterol analog with a pyrrole-linked BODIPY group to carbon-24 of cholesterol (B-P-Chol) (Fig. 1 *B*). We have assessed several membrane properties of B-P-Chol, including self-quenching propensity and partitioning between l_o and liquid-disordered (l_d) phases in model membranes, and compared them with B-Chol, the classical BODIPY-cholesterol derivative. We demonstrate using two-photon absorption at multiple polarization states that the orientation of the BODIPY-moiety depends on the membrane cholesterol content with larger probe restriction in the presence of cholesterol. Most importantly, we found that under physiological conditions the fluorophore in B-P-Chol is oriented parallel to lipid acyl chains, whereas in B-Chol it is oriented perpendicular to lipid acyl chains. Additionally, the orientation strength was much higher in B-Chol compared to B-P-Chol. The difference in orientation has a strong influence on the lateral diffusion constant of the Chol-analogs in the PM. Using fluorescence recovery after photobleaching (FRAP) and fluorescence correlation spectroscopy (FCS) we found that B-P-Chol diffuses significantly faster than B-Chol in cell membranes. The difference in lateral diffusion is most likely not caused by anomalous subdiffusion processes, as variable spot size FCS measurement on a stimulated emission depletion (STED) microscope (22,23) revealed normal Brownian motion for both probes. Potential reasons for these differences in light of current models of lateral diffusion in lipid membranes are discussed.

MATERIALS AND METHODS

Lipid reagents

BODIPY-cholesterol with the fluorophore attached to the central dipyrrometheneborone difluoride ring (B-Chol) was synthesized as described previously (11). The new Bodipy-cholesterol derivative (denoted here as B-P-Chol; see Fig. 1) in which the fluorophore is linked to C-24 of cholesterol at C-3 of a pyrrole ring of BODIPY was synthesized as described in the Supporting Material. 1-Palmitoyl-2-oleoyl-*sn*-glycero-3-phosphocholine (POPC), 1,2-dipalmitoyl-*sn*-glycero-3-phosphocholine (DPPC), 1,2-dioleoyl-*sn*-glycero-3-phosphocholine (DOPC), and a marker for the liquid-disordered phase, 1,1'-didodecyl-3,3,3′,3′-tetramethylindocarbocyanine perchlorate (DiIC12) were purchased from Avanti Polar Lipids (Alabaster, AL). All other chemicals were from Sigma Chemical (St. Louis, MO).

Measurements

The preparation of small, large, and giant unilamellar vesicles (SUVs, LUVs, and GUVs) as well as of supported bilayers, the culture of baby hamster kidney (BHK) and epithelial kidney (Vero) cells, spectroscopy of B-P-Chol in liposomes, multicolor wide field and two-photon excitation fluorescence microscopy, image analysis for polarization measurement, FRAP, and FCS as well as STED microscopy and its analysis are described in the Supporting Material.

RESULTS

Phase partitioning and fluorescence properties of B-P-Chol

An essential physical characteristic of any suitable fluorescent analog of cholesterol is the ability to partition

into the l_o phase in model membranes made of phospholipids with varying melting temperature. In GUVs one can induce l_o/l_d phase coexistence and find microscopically observable phase separation. Because cholesterol induces formation of the l_o phase, fluorescent sterols with a close resemblance of cholesterol should partition preferentially into the l_o phase. For example, the intrinsically fluorescent sterols, DHE and CTL have been shown to partition into the l_o phase with high preference (12,24). As shown in Fig. 1 *C*, B-P-Chol partitions preferentially into the l_o phase at the expense of the fluid l_d phase. As a marker for the liquid l_d phase, we chose DiIC12, because it localizes exclusively to that phase in GUVs made of DPPC/DOPC/cholesterol (1:1:1) (12). We found a very similar partition preference for B-P-Chol and B-Chol; quantification of BODIPY fluorescence for both probes in GUV images suggests a distribution of both sterols of ~1.5:1 to 2:1 between the l_o and l_d phases. To rule out that fluorophore self-quenching or similar photophysical nonlinearities (e.g., homoenergy transfer) compromise fluorescence measurements, we recorded emission spectra of B-P-Chol at varying concentrations in SUVs and LUVs (Fig. 1 *D*). Peak fluorescence of B-P-Chol at 515 nm was proportional to sterol probe concentration in liposomal membranes up to 10 mol %. Above that concentration, self-quenching of B-P-Chol was found, as inferred from a plateau of the probe's fluorescence emission for increasing mole fraction of the sterol in the bilayer (Fig. 1 *E*). Because we used only 0.5 mol % of the sterols in the partition experiments, self-quenching does not influence these measurements. We previously reported self-quenching of B-Chol in POPC liposomes at >3 mol % (12). Some BODIPY-tagged lipids have been observed to emit red-shifted fluorescence for increasing probe concentration in membranes (25). For example, a characteristic red-shifted emission peak was observed for BODIPY-tagged sphingolipids in bulk spectral measurements and subsequently used to determine probe concentration in model and cellular membranes (26). Interestingly, we did not find a red-shifted emission peak for B-Chol (12) or for B-P-Chol in similar bulk spectral measurements (Fig. 1 *D*). The molecular basis for the differences in emission spectra between various BODIPY-tagged lipids is not known. Similar as here for BODIPY-tagged cholesterol probes, no red-shifted emission could be detected in a recent study for a BODIPY analog of phosphatidylserine (27). In the absorption spectrum of B-Chol, we previously found a characteristic peak at 554 nm above the self-quenching probe concentration (12). This is characteristic for dark ground state dimers (excitons), which efficiently lower the probe fluorescence intensity, because fewer molecules become excited by the incident light. No such absorption peak was found in the spectrum of B-P-Chol (data not shown), suggesting that the quenching mechanisms of B-P-Chol and B-Chol are not identical.

Orientation of B-Chol and B-P-Chol in GUVs studied by polarization microscopy

An important parameter affecting membrane properties and fluorescence characteristics of any lipid probe is the molecular orientation of the attached fluorophore. For example, NBD-tagged phospholipids and sterols show artificially low membrane packing because of back-looping of the NBD moiety to the bilayer-water interface (28). The degree of this interfacial orientation of the NBD moiety was found to depend on the lipid composition and phase state of the bilayer (29). Fluorescence polarization microscopy is a well-known method to determine probe orientation in model and cell membranes. Use of two-photon excitation has several advantages for this purpose, including less scattering, intrinsic sectioning capability with ~300 and ~800 nm lateral and axial resolution, respectively, and, as we showed recently, high photostability of BODIPY-tagged cholesterol, making long-term observation and acquisition of several hundred frames without detectable photobleaching possible (17). For rod-like molecules (such as most laser dyes) the excitation probability is proportional to $\cos^4$ of the angle between the polarization plane of the excitation light and the main transition moment of the fluorophore. This gives a much higher extinction of the fluorophore than that found using single photon excitation, where the excitation probability is proportional to $\cos^2$ (30,31). By rotating the polarization plane of the incident light given by a femtosecond pulsed infrared laser over a full circle, we imaged B-Chol and B-P-Chol in GUVs prepared from POPC by polarized two-photon excitation microscopy (Fig. 2). Clearly, fluorescence of B-Chol follows the orientation of the incident light vector, $\boldsymbol{E}$, and is maximal when the incident light is oriented approximately parallel to the bilayer plane (Fig. 2 *A*; *white arrows* indicate the orientation of the incident light). A plot of fluorescence versus orientation of the incident light for a selected area on the top of the GUVs (*white box* in Fig. 2 *A*) shows two major peaks at ~0^0 and ~180°, respectively, and two minor peaks shifted by 90° relative to the large peaks (Fig. 2 *C*, *blue symbols*). Assuming a $\cos^4$ dependence, we fit the data to a two-component nonlinear cosine function of the form:

$$F(\theta) = A_1 \cdot \cos\left(\theta - \theta_0^1\right)^4 + A_2 \cdot \cos\left(\theta - \theta_0^2\right)^4 + F_0. \quad (1)$$

Here, θ is the rotation angle for the incident linearly polarized light vector, $\boldsymbol{E}$; $A_{1,2}$ are the peak amplitudes of the measured fluorescence and θ_0^1, θ_0^2 describe the orientation of the major fluorophore transition relative to the excitation vector, $\boldsymbol{E}$. The term F_0 describes background fluorescence or detector offset. We found that this function accurately describes the data (Fig. 2 *C*, *blue straight line*), whereas one with only one nonlinear cosine function missed the small peak (Fig. 2 *C*, *blue dashed line*). The dependence of B-P-Chol's fluorescence on the orientation of the incident light

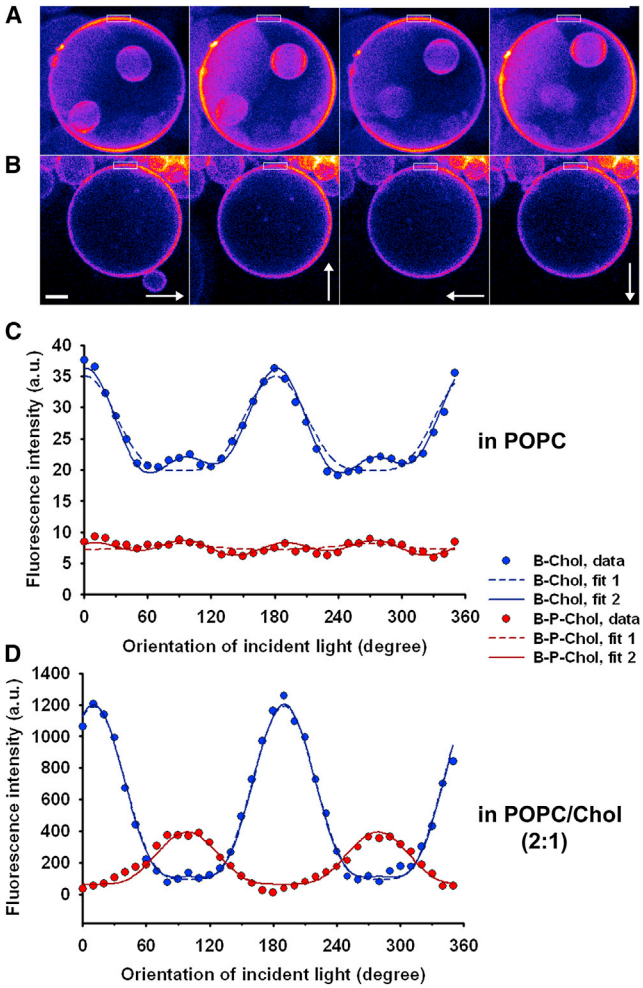

FIGURE 2 Two-photon fluorescence polarimetry of BODIPY orientation in model membranes. GUVs made of POPC and either B-Chol (*A*) or B-P-Chol (*B*) in mol percentages of 99:1 were imaged on a two-photon microscope with 10° rotation of the incident linearly polarized electric field vector, ***E***. The start position of ***E*** is horizontal, as indicated in the most left panel of *B*. Fluorescence intensities of both BODIPY-cholesterol probes were color-coded using a FIRE look-up table with high intensities in yellow/white and low intensities in blue. (*C*) Emission intensities were recorded for the small ROI on top of the GUVs (*rectangular white box* in *panels A*, *B*) for B-Chol (*blue symbols*) and B-P-Chol (*red symbols*) as a function of the orientation of ***E***. The straight blue and red lines show a fit of the data to Eq. 1. The dashed lines show a fit to Eq. 1 with the second amplitude, A_2 set to zero. (*D*) Fluorescence response of B-Chol (*blue symbols* – data, *blue straight line*, fit to Eq. 1 with $A_2 = 0$) and B-P-Chol (*red symbols* – data, *red straight line*, fit to Eq. 1 with $A_2 = 0$) in GUVs made of POPC, cholesterol (80:20 mol percentages). Scale bar = 5 μm.

is much less pronounced (Fig. 2, *B* and *C*, *red symbols*). This can be inferred from the much lower amplitude of fluorescence peaks compared to B-Chol (note that we verified independently, that the same amount of fluorophore was incorporated into both types of GUVs). The data for B-P-Chol were also accurately described by the model shown in Eq. 1 with peaks at the same orientations of incident light as found for B-Chol (i.e., 1.: 0–5°; 2.: ~90°; 3.: 180–190°; 4.: ~270°). However, the first and fourth peaks were much smaller than for B-Chol and of comparable height as the other two peaks. Thus, we found four maxima of fluorescence for comparable orientations of incident light for both BODIPY-tagged cholesterols in GUVs made of only POPC. The major difference is the fluorescence amplitude, which is large only for B-Chol's first and third fluorescence peak (i.e., at ~0^0 and ~180°). We can conclude that B-Chol gets preferentially excited when the incident light vector, ***E***, is parallel to the major transition axis in the BODIPY-moiety in B-Chol lying almost parallel to the bilayer normal in POPC membranes.

When cholesterol is added to a fluid membrane, the phospholipid acyl chains become ordered and more tightly packed. To test this influence on our fluorescent sterol probes, we performed the same measurements in POPC liposomes containing 30 mol % cholesterol. We observed a strong increase in the fluorescence amplitudes of the first and third peak for B-Chol (i.e., at ~0^0 and ~180°), although the second and fourth peak disappeared (Fig. 2 *D*, *blue symbols*). Fitting this data to the model in Eq. 1 revealed that one cosine^4 component is sufficient to describe the data, whereas adding the second term did not yield any improvement in fit quality (Fig. 2 *D*, *dashed* and *straight blue line*, lying on top of each other). From that fit, one can retrieve a mean orientation value but no information about the orientation strength of the fluorescent moieties. The latter can be inferred from a modified equation, where the fluorophore orientation is assumed to be normal distributed around its mean value θ^0 with a standard deviation σ. For two-photon excitation and one dominant probe orientation this gives the following expression for the fluorescence response (with the same notation as above, see the Supporting Material for derivation):

$$F(\theta) = \frac{3 \cdot A_1}{8} + \frac{A_1}{2} \cdot \cos\left(2\theta - 2\theta_0^1\right) \cdot \exp\left(-2\sigma^2\right) + \frac{A_1}{8} \cdot \cos\left(4\theta - 4\theta_0^1\right) \cdot \exp\left(-8\sigma^2\right) + F_0. \quad (2)$$

Fitting this function to the data of both BODIPY-tagged cholesterols in GUVs made of POPC/cholesterol gave a mean orientation of $\theta^0 = 10 \pm 0.08\ ^0$ and $\theta^0 = 98.8 \pm 0.3\ ^0$ relative to the incident field (i.e., perpendicular to the bilayer normal, see *arrows* in Fig. 2) for B-Chol and B-P-Chol, respectively (Fig. S1). The larger angle variation for B-P-Chol reflects the fact that the orientation strength of this cholesterol analog is significantly lower compared to B-Chol.

In two-photon excitation the transition moment is not a 3-component vector (as found for the one-photon case) but a 3 × 3 absorption tensor, because two absorption events have to take place simultaneously. The shape of this tensor is determined by the molecular geometry and sets the limits of observable polarized absorption. If this tensor is highly

asymmetric with only xx-elements being nonzero (defined by Cartesian indices along the molecule long axis), the photoselection is more pronounced than in one-photon excitation and follows a $\cos^4$-law. This is strictly speaking only found in rod-like molecules, such as linear polyenes, where each of the two photons uses a transition moment in the same direction (30,32). The BODIPY moiety belongs to the C_2 molecular symmetry group and therefore has two perpendicular orientations of preferred absorption (33). We found, however, only one dominating orientation in membranes condensed by adding cholesterol, and the $\cos^4$-function was able to fit the fluorescence response exactly (Fig. 2 *D*). For that reason and the sake of simplicity of the mathematical treatment of the data, we assumed only one transition moment in our analysis, as suggested previously for the BODIPY fluorophore (32) as well as for other not strictly rod-like probe molecules (34).

Orientation of B-Chol and B-P-Chol in cell membranes

We explored the photoselection effect further to determine the orientation of the BODIPY fluorophore attached to cholesterol in the PM of BHK cells. By rotating the electric field vector of the incident light around an axis perpendicular to the image (*xy*-) plane, we found that emission of B-Chol in plane membrane regions exactly followed the rotating excitation field. Due to the complex topography of cellular membranes, we have implemented a pixel-based analysis of the fluorescence response for this data (for details of that method, see the Supporting Material and (35)). Briefly, the orientation-dependent fluorescence is decomposed into Fourier components, and two ways of expressing the extracted physical parameters were used in images of GUVs (Fig. S2) and of cells (Fig. 3, Fig. S3 and Fig. S5). In the color-coded representation, the phase of the fluorescence response relative to the rotating incident vector is translated into probe orientation and expressed in the hue, saturation, and value color model (Fig. 3, *A* and *C*; see Fig. S2 *C* for the *color legend*). In the vector-coded representation, the amplitude (i.e., orientation strength) and phase (i.e., orientation angle) of the probe relative to the incident light vector are given as length and direction of small blue lines in each pixel position (e.g., in Fig. 3, *B* and *D*). Using this analysis, we found that the BODIPY group is oriented perpendicular to the bilayer normal for B-Chol in straight regions of the PM of living BHK cells (Fig. 3, *A* and *B*, and Fig. S3). In contrast, in regions with high surface ruffling, as on cell edges and surface protrusions, the fluorescence response to the rotating excitation vector was low. To determine whether this is a consequence of the local surface curvature or caused by a second population of nonoriented B-Chol molecules, we studied the fluorescence response in cells with disrupted actin cytoskeleton (Fig. 3, *C* and *D*). Treatment of cells for 30 min with 20 μM cytochalasin D induced formation of membrane blebs (3),

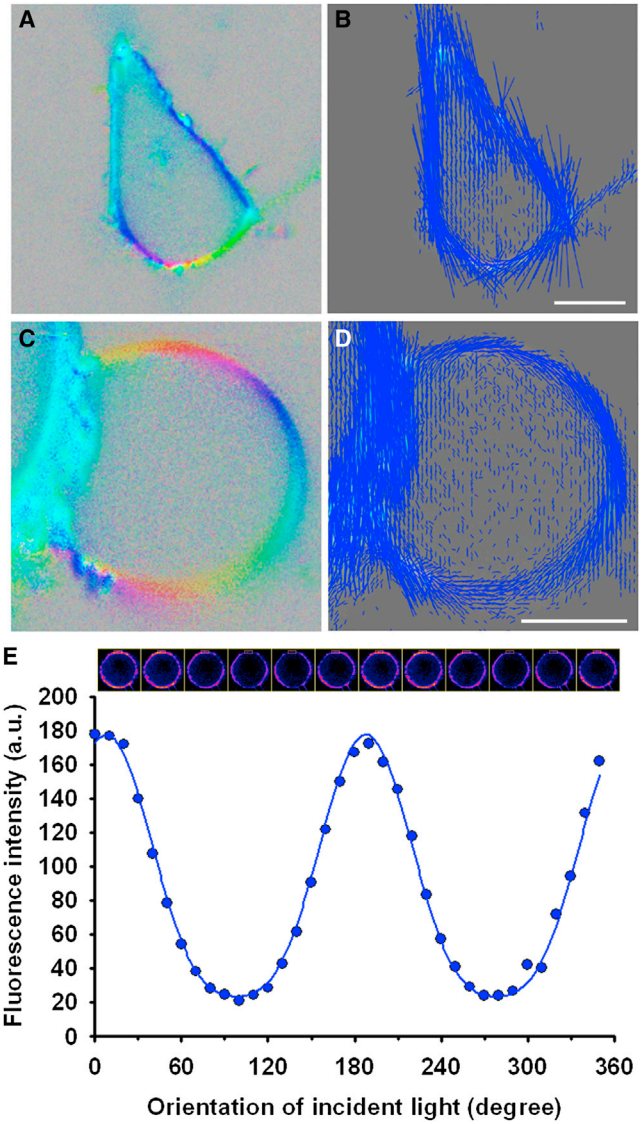

FIGURE 3 Two-photon fluorescence polarimetry of B-Chol in the PM of BHK cells. BHK cells were labeled with B-Chol from a B-Chol-CD complex as described in the Supporting Material. Cells were imaged on a two-photon microscope with 10° rotation of the incident linearly polarized electric field vector, ***E***. The start position of ***E*** is horizontal, as indicated in the legend to Fig. 2 *B*. (*A* and *B*) Show the color-coded (*A*) and vector-coded (*B*) presentation of the fluorescence response for intact cells. For *C* and *D*, cells were treated with 20 μM cytochalasin D for 30 min to disrupt the actin and induce bleb formation. The color-coded (*C*) and vector-coded (*D*) presentation of the fluorescence response is shown for a representative bleb. (*E*) Emission intensities were recorded for the small ROI on top of another cytochalasin-treated cell labeled with B-Chol (*blue symbols*) as a function of the orientation of ***E***. The straight blue line shows a fit of the data to Eq. 2. Scale bar = 5 μm.

and we found that the fluorescence response of B-Chol in these blebs is comparable to that in GUVs made of POPC/cholesterol (compare Fig. S2 *A* and Fig. 3, *C* and *D*). Extracting the intensity of B-Chol emission as a function of the orientation of the incident field for a representative cytochalasin-treated cell and fitting the fluorescence

response to Eq. 2 gave a mean orientation of $\theta^0 = 6.21 \pm 0.221\ ^0$ (Fig. 3 *E*). From this result it can be concluded that the angle and strength of the orientation of the BODIPY moiety in B-Chol in cell membranes is comparable to that determined for GUVs containing 30 mol % cholesterol with a strongly confined, almost perpendicular orientation of the flurophore relative to the bilayer normal. In highly convoluted surface regions the orientation of the BODIPY flurophore attached to cholesterol's side chain seems to have no preferred direction but follows the rough surface topography, as also confirmed in measurements of the same cell at varying focus positions (see Fig. S3). Accordingly, in ruffles there is no preferred direction in which the incident excitation light can excite B-Chol, resulting in small, randomly oriented molecular directors **c**. By two-photon time-lapse microscopy, we observed that surface ruffles containing B-Chol are dynamic entities constantly protruding and retracting, thereby changing the local surface topology on a timescale of several minutes (see Fig. S4). When doing the same polarization measurements with B-P-Chol, we found a very low fluorescence response to the rotating incident excitation vector as concluded from the vector- and color-coded representation (Fig. S5). There was a slight tendency toward an orientation of the BODIPY-group of B-P-Chol parallel to the membrane normal, especially after actin disruption (compare Fig. S5 *A*, *B* and *C*, *D*). This result is again largely in agreement with the data of B-P-Chol orientation in GUVs prepared from POPC/cholesterol. It suggests some alignment of the fluorophore in B-P-Chol with the direction of the fatty acyl chains (compare Fig. S2 and Fig. S5). We conclude that the fluorescent moiety in B-P-Chol experiences much less structural confinement in model and cell membranes than the BODIPY group in B-Chol.

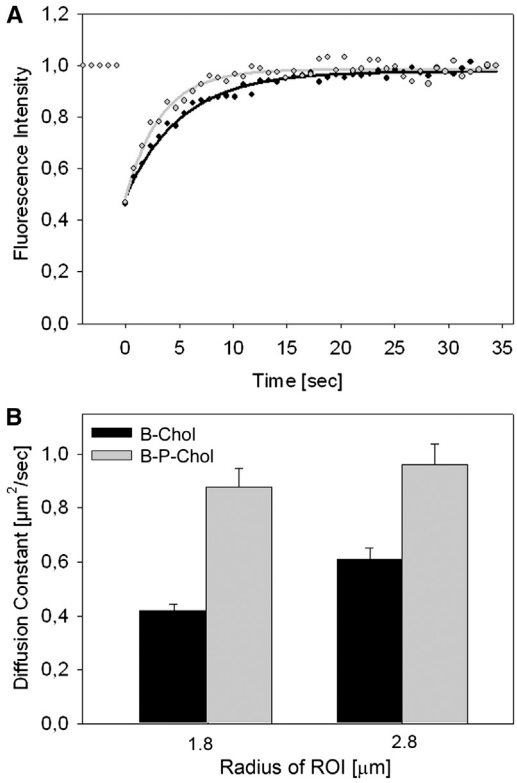

FIGURE 4 FRAP measurement of B-Chol and B-P-Chol in the PM of BHK-cells. FRAP experiments were performed on a Zeiss LSM510 confocal microscope in living BHK cells, as described in the Supporting Material. (*A*) Fluorescence recovery curves for FRAP in a circular ROI with radius $r = 2.8\ \mu$m for both BODIPY-cholesterol analogs. Black and gray symbols show the mean of five measurements for B-Chol and B-P-Chol, respectively. The black and gray lines show the fit of Eq. S2 for B-Chol and B-P-Chol, respectively. (*B*) The FRAP experiment was performed for circular ROIs with radii of 1.8 and 2.8 μm. The bar plot shows the diffusion constants for the B-Chol (*black*) and B-P-Chol (*gray*) for each experiment with error bars of $\pm$ one standard error.

Diffusion of B-Chol and B-P-Chol in model and cell membranes measured by FRAP and FCS

To test whether the angle and strength of fluorophore orientation in the two BODIPY-tagged cholesterol probes affect their lateral diffusion, we first performed FRAP measurements in the PM of BHK cells labeled with either B-Chol or B-P-Chol (Fig. 4). In the FRAP experiment a region of interest (ROI) in the PM is bleached and the fluorescence recovery is imaged over time. For a detailed FRAP protocol see the Supporting Material. Fig. 4 *A* shows the mean of five fluorescence recovery curves for a circular ROI with radius 2.8 μm and the fits of Eq. S2 in blue and red for B-Chol and B-P-Chol, respectively. If the diffusing probes are not trapped in microscopic domains of the PM, the size of the bleached area should not affect the diffusion constant (36,37). To test this, we performed FRAP experiments with ROIs with radii of 1.8 and 2.8 μm, respectively. As shown in Fig. 4 *B*, the size of the bleach ROI had no effect on the measured diffusion constants, whereas B-P-Chol diffused almost twice as fast as B-Chol, i.e., $D_{B\text{-}P\text{-}Chol} = 0.8\text{–}1.0\ \mu m^2/s$ compared to $D_{B\text{-}Chol} = 0.5\ \mu m^2/s$. BODIPY-tagged cholesterol including B-Chol has been shown to move by vesicular and nonvesicular transport between PM and intracellular compartments (12,17). During the laser-based bleaching in a FRAP experiment on a confocal microscope significant photodestruction takes place above and below the focal plane (38). For example, we have recently shown in experiments on fixed cells and in three-dimensional reaction-diffusion simulations that a 63× objective with NA = 1.4 as used here causes photobleaching in a cone shape up to several micrometers beyond the depth of field (see Fig. S2 and S3 in (39)). Because B-Chol diffuses rather slowly in the cytoplasm of mammalian cells (17), it could become necessary to include a cytoplasmic diffusion term into the FRAP analysis. To do so, we have applied the extended FRAP model developed by Berkovich et al. (40) and found an almost identical goodness of fit as with the simple FRAP model (not shown). However,

the estimated parameters including diffusion constants in the PM and cytoplasm and the on-/off-rates between both compartments were associated with a large uncertainty, which led us to conclude that the simple FRAP model given in Eq. S2 is sufficient to accurately describe movement of BODIPY-tagged cholesterol probes in the PM of BHK cells.

To determine the lateral mobility of both BODIPY-tagged cholesterol probes in lipid membranes in more detail, we used FCS. FCS measures the mean transit time of single molecules diffusing through a confocal observation volume. The lateral diffusion constant of the probe can be calculated with high statistical precision by FCS when the size of the confocal volume is known. To determine if the different molecular orientations of B-Chol and B-P-Chol are reflected in the lateral diffusion of both sterol probes, we conducted FCS measurements in model membranes and in live cell membranes (Fig. 5 *A*). We obtained a lateral diffusion constant of D = 3.2 $\mu m^2/s$ for both probes in cholesterol free supported DOPC membranes. In supported membranes made of POPC and 30 mol % cholesterol the lateral diffusion of both cholesterol probes was reduced by a factor of 1.9 to D = 1.7 $\mu m^2/s$. Again, as for the cholesterol-free membranes, we found no significant difference in lateral mobility between the two sterol probes. Finally, we incorporated B-Chol and B-P-Chol in the PM of cultured Vero epithelial kidney cells and determined the lateral diffusion constant with FCS. In agreement with the FRAP experiments in BHK-cells, we found that B-P-Chol diffused significantly faster with $D_{B\text{-}P\text{-}Chol} = 2.6\ \mu m^2/s$ compared to B-Chol, which diffused with $D_{B\text{-}Chol} = 1.7\ \mu m^2/s$. Although the difference in diffusion constants $D_{B\text{-}P\text{-}Chol}/D_{B\text{-}P\text{-}Chol} \approx 1.6$ was roughly the same in BHK and Vero cells, the absolute values differed by a factor of ~3–3.5. This is not surprising, because the absolute diffusion constants can vary between different cell types (5). Even though we performed FCS measurement as soon as possible after staining the PM (2–5 min), we observed that a fraction of the probes had already entered the cytosol of the cells. To exclude the possibility that the difference in lateral diffusion of the two cholesterol analogs was caused by a different partitioning into the cytoplasm or organelle membranes, we produced PM sheets removing the cytosol and inner membranes. In membrane sheets the difference in lateral diffusion of the two cholesterol analogs was in the same range as measured in the PM of intact living cells (see Fig. S6). This supports the conclusion that B-P-Chol indeed moves significantly faster in the PM compared to B-Chol and rules out that a cytoplasmic component of sterol diffusion contributes to the measured differences in PM diffusion.

Probing anomalies in lateral diffusion of B-Chol and B-P-Chol in cell membranes with STED-FCS

To test whether the observed difference between the lateral diffusion of B-Chol and B-P-Chol in the PM (FRAP and confocal FCS) was caused by anomalous subdiffusion processes, for example due to transient trapping of the sterols in subregions of the PM, we applied superresolution STED-FCS (22,23,41). Applying FCS on a STED microscope allows determination of the values of the apparent diffusion coefficient D for different observation spot sizes (tuned for example by the intensity of the STED laser) below the diffraction limit of ~200 nm of conventional optical microscopy (5,23,41). The dependency of D on the diameter d of the observation spots indicates whether diffusion is hindered or not (5,41,42). Constant values of $D(d)$ demonstrate free Brownian diffusion, although a decrease of D toward smaller observation sizes shows hindered diffusion, for example, due to transient interactions with relatively slow moving or immobilized molecules (trapping) (5,43). In our measurements we used a continuous-wave 577 nm STED laser. We set the power of the STED laser to 80 mW and varied the size of the observation spot by gated STED-FCS. In gated STED-FCS, the combination of pulsed excitation and gated detection realizes a reduction of the diameter d of the effective observation spot with increasing temporal shift of the detection window (time gate) with respect to the excitation pulse (44). We first checked whether gated STED-FCS is applicable to the Bodipy-cholesterol probes. To this end, we determined the average transit time of both, B-Chol and B-P-Chol, diffusing in supported lipid bilayers made of POPC + 30 mol % cholesterol for different time gates (Fig. 5 *C*). We could clearly observe a reduction of the transit time with gating position, allowing us to calibrate the dependency of the effective diameter d of the observation spot on the time gate, which was the same for both B-Chol and B-P-Chol. Next, we determined the dependency $D(d)$ for both cholesterol analogs in the PM of Vero cells from diffraction-limited $d = 190$ nm down to $d = 80$ nm (Fig. 5 *E*). Interestingly, the dependency $D(d)$ was almost constant for both analogs, indicating close to free diffusion with only weak transient interactions (or trapping). Accordingly, the difference in lateral diffusion between the probes remained constant when the observation area was decreased, with B-P-Chol diffusing 1.7-fold faster than B-Chol. Furthermore, as shown in Fig. 5 *C*, the extrapolated intercept of the mean transit time for focal areas $\rightarrow 0\ \mu m$ was close to zero for B-Chol and B-P-Chol in accordance with free diffusion of both Bodipy-cholesterol probes (42). Thus, the STED-FCS results show that the difference in lateral diffusion between B-P-Chol and B-Chol is not caused by anomalous subdiffusion processes due to transient molecular interactions.

DISCUSSION

In this study, we introduced a BODIPY-tagged cholesterol analog with the dye being attached to the cholesterol side chain via one of BODIPY's pyrrole rings (B-P-Chol,

Fig. 1 *B*). We demonstrated by two-photon fluorescence polarimetry that the fluorophore in B-P-Chol had a tendency to be aligned along the fatty acyl chains in both, cholesterol containing model membranes and in cell membranes (compare Fig. 2 *B* and Figs. S4, S5). In contrast, B-Chol, the classical BODIPY-tagged cholesterol in which the fluorophore is attached via the *meso*-carbon of the dipyrromethene moiety to cholesterol's side chain, was found to orient its fluorescent group perpendicular to the fatty acyl chains with a much stronger confinement than B-P-Chol in both model and cell membranes (compare Figs. 2 and 3 with Fig. S2 and Fig. S3). The difference in orientation of both probes was not found in cholesterol-free model membranes (see Fig. 2), where B-P-Chol and B-Chol showed a bimodal distribution, as previously reported for other BODIPY-tagged lipid probes (45,46). Interestingly, recent MD simulations also found a perpendicular orientation of the BODIPY moiety of B-Chol in DPPC bilayers with an additional small population of back-looped fluorophores oriented almost parallel to the membrane normal (10). Time-resolved anisotropy measurements of B-Chol in GUVs have confirmed an orientation of the BODIPY group perpendicular to the membrane normal (13). Additionally, the fluorescence anisotropy of B-Chol showed a multiexponential decay pattern in these measurements, which was likely due to several rotational modes of the sterol probe in the bilayer (13). B-Chol distends its fluorophore toward the center of the bilayer, as shown by quenching experiments with spin labels as well as by ^{2}H-NOESY NMR experiments (47). Interestingly, despite its preferred partition into the cholesterol-induced l_o phase (see Fig. 1, *C* and *D*, and (12–15)), B-Chol did not induce acyl-chain ordering in liposomes in a comparable manner to cholesterol (47). The attached BODIPY moiety will likely slow down the rotation of cholesterol's alkyl chain from a mean correlation time of <1 ns (48) to at least 5 ns (13). This will clearly affect some of the physico-chemical properties of the linked cholesterol. Based on our two photon polarimetry experiments, we propose that the BODIPY moiety in B-Chol occupies more space perpendicular to the bilayer normal, which is why it is sterically hindered in its movement and thereby more confined than that of B-P-Chol. A larger free volume for the BODIPY moiety in B-P-Chol is suggested by the lower fluorescence response in the two-photon polarimetry measurements and by the higher onset of fluorophore self-quenching in liposomes for B-P-Chol (i.e., 10 mol %, Fig. 1, *D* and *E*), than for B-Chol (i.e., 3 mol % (12)). One can therefore speculate that the sterol orientation in B-P-Chol is less disturbed by the attached fluorophore than in B-Chol. Consequently, the sterol might be less tilted favoring a more cholesterol-like behavior for B-P-Chol than for B-Chol. Surprisingly, the high protein density in the PM did not change the relative orientation of the BODIPY group in the cholesterol analogs compared to protein free model membranes. This, however, does not exclude the possibility that the rotational dynamics of the BODIPY moiety is different in the protein containing PM compared to model membranes for both cholesterol probes, something which might be explored in future systematic studies (13,47).

The different orientation of the BODIPY-fluorophore did not affect the lateral diffusion of both sterol analogs in model membranes. In supported model membranes made of POPC and 30 mol % cholesterol, the lateral diffusion of both cholesterol probes measured by FCS was comparable and reduced by almost twofold compared to membranes made of DOPC without cholesterol (see Fig. 5 *A*). For B-Chol, this is in line with earlier FCS measurements on GUVs showing that the analog diffuses significantly slower in the cholesterol-rich l_o phase (i.e., 4.98 $\mu m^2/s$) compared to the cholesterol-poor l_d phase (i.e., 7.23 $\mu m^2/s$) (13). Although the lipid composition of the GUVs differed somehow in the study by Ariola et al. from that used here (i.e., ternary mixtures of DOPC/SM/cholesterol were used in the study by Ariola et al. (13)), the overall faster diffusion of B-Chol in GUVs in that study compared to our experiments with supported bilayers is likely a consequence of the friction induced by the solid support when using supported membranes, as thoroughly studied previously (49). The different orientation of the BODIPY-fluorophore had a profound effect on the motion of both BODIPY-cholesterol probes in the PM of living cells. Using FRAP and FCS in two different cell types (Vero and BHK cells), we found a 1.5- to 1.8-fold slower diffusion for B-P-Chol compared to B-Chol (see Figs. 4 and 5). Furthermore, STED-FCS measurements confirmed the results obtained by FRAP and FCS and showed that lateral diffusion of B-Chol and B-P-Chol was not hindered in the PM (see Fig. 5, *C* and *D*, and Fig. S6). The observed relatively free diffusion of the cholesterol analogs is surprising, because cholesterol is supposed to be highly interactive in the PM of living cells, facilitating various molecular interactions (2,5,41). Either the fluorescent BODIPY-tagged analogs, in contrast to their endogenous counterparts, were not involved in such complexes or the transient interactions of cholesterol are weak and characterized by large off-rates compared to on-rates resulting in almost constant $D(d)$ dependencies, as previously determined for fluorescent phosphoethanolamine lipids using STED-FCS (5,41). In fact, it has been shown in simulations, that equilibration of a diffusing species between a finite hierarchy of binders will result in normal diffusion at all timescales (43). However, given that both sterol probes diffuse freely in the PM of living cells, why is there a difference in diffusion constants? In general, lateral diffusion of lipids and small hydrophobic molecules in membranes has been described in the framework of the free volume theory first proposed by Cohen and Turnbull (50), later extended by Macedo and Litovitz by taking Eyrings transition state theory into account (51) and applied in the context of lipid membranes by Almeida,

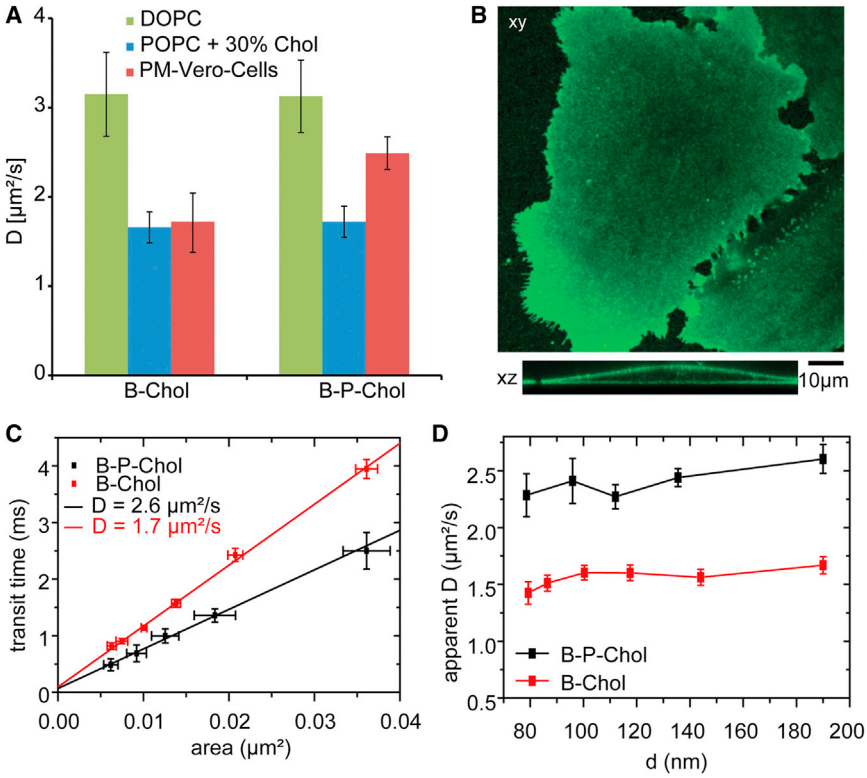

FIGURE 5 FCS and STED-FCS of B-Chol and B-P-Chol in model and cell membranes. (*A*) Diffusion coefficients *D* of B-Chol and B-P-Chol in supported lipid bilayers (DOPC: one-component DOPC; POPC + 30% Chol: two-component system POPC and 30 mol% cholesterol) and in the PM of living Vero cells (PM-Vero-Cells) as determined by (*confocal*) FCS. (*B*) Confocal fluorescence scanning image of a Vero cell labeled with B-P-Chol (*upper panel*: *xy* scan; *lower panel*: *xz* scan). (*C* and *D*) STED-FCS data of B-Chol (*red*) and B-P-Chol (*black*) diffusion in the PM of living Vero cells: average transit time through the observation spot (*C*) and apparent diffusion coefficient *D* (*D*) determined from FCS measurements at different sizes of the observation spot (*C*, area and *D*, diameter *d*). A linear transit-time (*area*) dependency and constant *D*(*d*) values reveal almost free diffusion of both probes with absolute value of *D* indicated in the panels.

Vaz, and co-workers (52). Using FCS, the dependence of lateral diffusion coefficients of fluorescent lipid probes on the mean molecular area has been verified in phospholipid monolayers even in quantitative agreement with the free volume theory (53). The basic idea of the free volume model is that diffusing probes can only step forward from their initial position (i.e., hop), if i), sufficient free volume in the bilayer is transiently generated by thermally or otherwise driven local density fluctuations and ii), the diffusing molecule acquires enough energy to break away its immediate neighbors (54). Because both BODIPY-tagged sterols move freely in the PM, we assume that the second condition is fulfilled for B-Chol and B-P-Chol. Recent extensions of this model suggested by MD simulations take the highly heterogeneous lateral pressure profile in membranes into account (55,56). These simulations show that the free volume is not isotropically distributed but appears transiently in the form of ellipsoidal voids mostly oriented along the fatty acyl chains in a cholesterol-dependent manner (55,56). Membrane-embedded proteins have been found to further lower the free volume and to compress the immediately surrounding bilayer and thereby to lower the diffusion rates of membrane lipids (57,58). Proteins with hydrophobic residues exceeding the bilayer thickness can often deform the bilayer such that it gets locally thicker with a coherence length of 1.5–2 nm (59). Lipids with longer hydrophobic tails tend to cluster around such proteins without binding to them, although at the same time their acyl chains order underneath the headgroup and disorder close to the bilayer center (59,60). In addition, extended MD simulations suggest that these annulus lipids correlate their lateral movement with that of the embedded protein and therefore diffuse much slower than lipids further apart (60,61). In light of these results, we speculate that B-Chol due to its BODIPY-moiety stretching into the bilayer center is more anchored and slightly longer than B-P-Chol. This causes a higher tendency of B-Chol to occupy places adjacent to proteins to avoid its hydrophobic mismatch but also to account for its lower mobility parallel to the bilayer normal (21). As a consequence, B-Chol comes to diffuse more frequently in concert with the much larger membrane-embedded proteins resulting on average in the measured lower diffusion constant compared to B-P-Chol in the PM. Further studies involving NMR and fluorescence spectroscopy as well as simulations of membrane proteins in the presence of the fluorescent sterols might be useful to explore this possibility further. Alternatively, it is possible that B-Chol and B-P-Chol have a different preference for the outer versus inner leaflet of the PM. The cytoplasmic leaflet is rich in the aminophospholipids, phosphatidylserine and phosphatidylethanolamine. The inner leaflet is generally considered as being more fluid than the outer leaflet; the latter being more enriched in sphingolipids with saturated acyl chains (62). Accordingly, the outer leaflet is likely more packed and lateral diffusion of lipids including sterols should be faster in the inner leaflet of the PM. Both predictions have been confirmed in model membrane systems mimicking the outer and inner leaflet lipid composition,

respectively (63–65). Interestingly, the intrinsically fluorescent close cholesterol mimics DHE and CTL have been found to reside mostly in the cytoplasmic leaflet of the PM in fibroblasts and macrophages (66–68). By assuming that B-P-Chol is more enriched in the inner leaflet of the PM than B-Chol, one can easily explain its faster diffusion in the PM and PM sheets compared to B-Chol. Different transbilayer distribution of both BODIPY-cholesterol analogs could even explain why B-P-Chol diffuses faster in the PM than in model membranes containing cholesterol (see Fig. 5 *A*). Future studies in our lab will focus on determining the transbilayer distribution and mobility of B-Chol and B-P-Chol in living cells.

SUPPORTING MATERIAL

Seven figures, twelve equations, six schemes, references (69–72) and supplementary data are available at http://www.biophysj.org/biophysj/supplemental/S0006-3495(13)01079-5.

D.W. acknowledges funding from the Lundbeck, Villum and NovoNordisk foundations, C.E. and A.H. from the Deutsche Forschungsgemeinschaft (DFG) via the SFB937.A.H. and C.E. acknowledge continuous support by Prof. Stefan Hell. The Danish Molecular Biomedical Imaging Center (DaMBIC) and its director Prof. Luis Bagatolli are acknowledged for making the two-photon microscope available.

REFERENCES

1. Munro, S. 2003. Lipid rafts: elusive or illusive? *Cell.* 115:377–388.
2. Simons, K., and E. Ikonen. 1997. Functional rafts in cell membranes. *Nature*. 387:569–572.
3. Wüstner, D. 2007. Plasma membrane sterol distribution resembles the surface topography of living cells. *Mol. Biol. Cell.* 18:211–228.
4. Wüstner, D., and N. J. Faergeman. 2008. Spatiotemporal analysis of endocytosis and membrane distribution of fluorescent sterols in living cells. *Histochem. Cell Biol.* 130:891–908.
5. Mueller, V., C. Ringemann, …, C. Eggeling. 2011. STED nanoscopy reveals molecular details of cholesterol- and cytoskeleton-modulated lipid interactions in living cells. *Biophys. J.* 101:1651–1660.
6. Jaqaman, K., H. Kuwata, …, S. Grinstein. 2011. Cytoskeletal control of CD36 diffusion promotes its receptor and signaling function. *Cell.* 146:593–606.
7. Gowrishankar, K., S. Ghosh, …, M. Rao. 2012. Active remodeling of cortical actin regulates spatiotemporal organization of cell surface molecules. *Cell.* 149:1353–1367.
8. Scheidt, H. A., P. Müller, …, D. Huster. 2003. The potential of fluorescent and spin-labeled steroid analogs to mimic natural cholesterol. *J. Biol. Chem.* 278:45563–45569.
9. Mukherjee, S., X. Zha, …, F. R. Maxfield. 1998. Cholesterol distribution in living cells: fluorescence imaging using dehydroergosterol as a fluorescent cholesterol analog. *Biophys. J.* 75:1915–1925.
10. Hölttä-Vuori, M., R. L. Uronen, …, E. Ikonen. 2008. BODIPY-cholesterol: a new tool to visualize sterol trafficking in living cells and organisms. *Traffic.* 9:1839–1849.
11. Li, Z., E. Mintzer, and R. Bittman. 2006. First synthesis of free cholesterol-BODIPY conjugates. *J. Org. Chem.* 71:1718–1721.
12. Wüstner, D., L. M. Solanko, …, A. Herrmann. 2011. Quantitative assessment of sterol traffic in living cells by dual labeling with dehydroergosterol and BODIPY-cholesterol. *Chem. Phys. Lipids.* 164:221–235.
13. Ariola, F. S., Z. Li, …, A. A. Heikal. 2009. Membrane fluidity and lipid order in ternary giant unilamellar vesicles using a new bodipy-cholesterol derivative. *Biophys. J.* 96:2696–2708.
14. Sezgin, E., I. Levental, …, P. Schwille. 2012. Partitioning, diffusion, and ligand binding of raft lipid analogs in model and cellular plasma membranes. *Biochim. Biophys. Acta.* 1818:1777–1784.
15. Shaw, J. E., R. F. Epand, …, C. M. Yip. 2006. Correlated fluorescence-atomic force microscopy of membrane domains: structure of fluorescence probes determines lipid localization. *Biophys. J.* 90:2170–2178.
16. Jansen, M., Y. Ohsaki, …, E. Ikonen. 2011. Role of ORPs in sterol transport from plasma membrane to ER and lipid droplets in mammalian cells. *Traffic.* 12:218–231.
17. Lund, F. W., M. A. Lomholt, …, D. Wüstner. 2012. Two-photon time-lapse microscopy of BODIPY-cholesterol reveals anomalous sterol diffusion in Chinese hamster ovary cells. *BMC Biophys.* 5:20.
18. Ipsen, J. H., O. G. Mouritsen, and M. Bloom. 1990. Relationships between lipid membrane area, hydrophobic thickness, and acyl-chain orientational order. The effects of cholesterol. *Biophys. J.* 57:405–412.
19. Aittoniemi, J., T. Róg, …, I. Vattulainen. 2006. Tilt: major factor in sterols' ordering capability in membranes. *J. Phys. Chem. B.* 110:25562–25564.
20. Weisz, K., G. Gröbner, …, G. Kothe. 1992. Deuteron nuclear magnetic resonance study of the dynamic organization of phospholipid/cholesterol bilayer membranes: molecular properties and viscoelastic behavior. *Biochemistry.* 31:1100–1112.
21. Gliss, C., O. Randel, …, T. Bayerl. 1999. Anisotropic motion of cholesterol in oriented DPPC bilayers studied by quasielastic neutron scattering: the liquid-ordered phase. *Biophys. J.* 77:331–340.
22. Klar, T. A., S. Jakobs, …, S. W. Hell. 2000. Fluorescence microscopy with diffraction resolution barrier broken by stimulated emission. *Proc. Natl. Acad. Sci. USA*. 97:8206–8210.
23. Kastrup, L., H. Blom, …, S. W. Hell. 2005. Fluorescence fluctuation spectroscopy in subdiffraction focal volumes. *Phys. Rev. Lett.* 94:178104.
24. Baumgart, T., G. Hunt, …, G. W. Feigenson. 2007. Fluorescence probe partitioning between Lo/Ld phases in lipid membranes. *Biochim. Biophys. Acta.* 1768:2182–2194.
25. Marks, D. L., R. Bittman, and R. E. Pagano. 2008. Use of Bodipy-labeled sphingolipid and cholesterol analogs to examine membrane microdomains in cells. *Histochem. Cell Biol.* 130:819–832.
26. Chen, C. S., O. C. Martin, and R. E. Pagano. 1997. Changes in the spectral properties of a plasma membrane lipid analog during the first seconds of endocytosis in living cells. *Biophys. J.* 72:37–50.
27. Kay, J. G., M. Koivusalo, …, S. Grinstein. 2012. Phosphatidylserine dynamics in cellular membranes. *Mol. Biol. Cell.* 23:2198–2212.
28. Chattopadhyay, A., and E. London. 1987. Parallax method for direct measurement of membrane penetration depth utilizing fluorescence quenching by spin-labeled phospholipids. *Biochemistry.* 26:39–45.
29. Raghuraman, H., S. Shrivastava, and A. Chattopadhyay. 2007. Monitoring the looping up of acyl chain labeled NBD lipids in membranes as a function of membrane phase state. *Biochim. Biophys. Acta.* 1768:1258–1267.
30. Callis, P. R. 1997. The theory of two-photon induced fluorescence anisotropy. *In* Topics in Fluorescence Spectroscopy: Nonlinear and Two-Photon-Induced Fluorescence, *Vol. 5*. Plenum, New York, pp. 1–42.
31. Brasselet, S., P. Ferrand, …, A. Gasecka. 2013. Imaging Molecular Order in Cell Membranes by Polarization-Resolved Fluorescence Microscopy. Berlin Heidelberg, Springer.
32. Benninger, R. K., B. Önfelt, …, P. M. French. 2005. Fluorescence imaging of two-photon linear dichroism: cholesterol depletion disrupts molecular orientation in cell membranes. *Biophys. J.* 88:609–622.
33. Opanasyuk, O., L. Ryderfors, …, L. B. Johansson. 2009. Two-photon excited fluorescence depolarization and electronic energy migration within donor-donor pairs. *Phys. Chem. Chem. Phys.* 11:7152–7160.

34. Farkas, E. R., and W. W. Webb. 2010. Multiphoton polarization imaging of steady-state molecular order in ternary lipid vesicles for the purpose of lipid phase assignment. *J. Phys. Chem. B.* 114:15512–15522.
35. Bernchou, U., J. Brewer, …, A. C. Simonsen. 2009. Texture of lipid bilayer domains. *J. Am. Chem. Soc.* 131:14130–14131.
36. Yechiel, E., and M. Edidin. 1987. Micrometer-scale domains in fibroblast plasma membranes. *J. Cell Biol.* 105:755–760.
37. Yguerabide, J., J. A. Schmidt, and E. E. Yguerabide. 1982. Lateral mobility in membranes as detected by fluorescence recovery after photobleaching. *Biophys. J.* 40:69–75.
38. Weiss, M. 2004. Challenges and artifacts in quantitative photobleaching experiments. *Traffic.* 5:662–671.
39. Wüstner, D., L. M. Solanko, …, M. A. Lomholt. 2012. Quantitative fluorescence loss in photobleaching for analysis of protein transport and aggregation. *BMC Bioinformatics.* 13:296.
40. Berkovich, R., H. Wolfenson, …, M. Urbakh. 2011. Accurate quantification of diffusion and binding kinetics of non-integral membrane proteins by FRAP. *Traffic.* 12:1648–1657.
41. Eggeling, C., C. Ringemann, …, S. W. Hell. 2009. Direct observation of the nanoscale dynamics of membrane lipids in a living cell. *Nature.* 457:1159–1162.
42. Wawrezinieck, L., H. Rigneault, …, P.-F. Lenne. 2005. Fluorescence correlation spectroscopy diffusion laws to probe the submicron cell membrane organization. *Biophys. J.* 89:4029–4042.
43. Saxton, M. J. 2007. A biological interpretation of transient anomalous subdiffusion. I. Qualitative model. *Biophys. J.* 92:1178–1191.
44. Vicidomini, G., G. Moneron, …, S. W. Hell. 2011. Sharper low-power STED nanoscopy by time gating. *Nat. Methods.* 8:571–573.
45. Kaiser, R. D., and E. London. 1998. Determination of the depth of BODIPY probes in model membranes by parallax analysis of fluorescence quenching. *Biochim. Biophys. Acta.* 1375:13–22.
46. Armendariz, K. P., H. A. Huckabay, …, R. C. Dunn. 2012. Single molecule probes of membrane structure: orientation of BODIPY probes in DPPC as a function of probe structure. *Analyst (Lond.).* 137:1402–1408.
47. Milles, S., T. Meyer, …, P. Müller. 2013. Organization of fluorescent cholesterol analogs in lipid bilayers - lessons from cyclodextrin extraction. *Biochim. Biophys. Acta.* 1828:1822–1828.
48. Taylor, M. G., T. Akiyama, …, I. C. Smith. 1982. Direct observation of the properties of cholesterol in membranes by deuterium NMR. *Chem. Phys. Lipids.* 31:359–379.
49. Przybylo, M., J. Sýkora, …, M. Hof. 2006. Lipid diffusion in giant unilamellar vesicles is more than 2 times faster than in supported phospholipid bilayers under identical conditions. *Langmuir.* 22:9096–9099.
50. Cohen, M. H., and D. Turnbull. 1959. Molecular transport in liquids and glasses. *J. Chem. Phys.* 31:1164–1169.
51. Macedo, P. B., and T. A. Litovitz. 1965. On the relative roles of free volume and activation energy in the viscosity of liquids. *J. Chem. Phys.* 42:245–256.
52. Almeida, P. F., W. L. Vaz, and T. E. Thompson. 1992. Lateral diffusion in the liquid phases of dimyristoylphosphatidylcholine/cholesterol lipid bilayers: a free volume analysis. *Biochemistry.* 31:6739–6747.
53. Gudmand, M., M. Fidorra, …, T. Heimburg. 2009. Diffusion and partitioning of fluorescent lipid probes in phospholipid monolayers. *Biophys. J.* 96:4598–4609.
54. Chung, H. S. 1966. On the Macedo-Litovitz hybrid equation for liquid viscosity. *J. Chem. Phys.* 44:1362–1364.
55. Xiang, T. 1999. Translational diffusion in lipid bilayers: dynamic free-volume theory and molecular dynamics simulations. *J. Phys. Chem. B.* 103:385–394.
56. Falck, E., M. Patra, …, I. Vattulainen. 2004. Impact of cholesterol on voids in phospholipid membranes. *J. Chem. Phys.* 121:12676–12689.
57. Lundbæck, J. A., and O. S. Andersen. 2012. Cholesterol regulation of membrane protein function by changes in bilayer physical properties - an energetic perspective. *In* Cholesterol regulation of ion channels and receptors. I. a. B. F. Levitan, editor. John Wiley & Sons, pp. 27–44.
58. O'Leary, T. J. 1987. Lateral diffusion of lipids in complex biological membranes. *Proc. Natl. Acad. Sci. USA.* 84:429–433.
59. Jensen, M. O., and O. G. Mouritsen. 2004. Lipids do influence protein function-the hydrophobic matching hypothesis revisited. *Biochim. Biophys. Acta.* 1666:205–226.
60. Niemelä, P. S., M. S. Miettinen, …, I. Vattulainen. 2010. Membrane proteins diffuse as dynamic complexes with lipids. *J. Am. Chem. Soc.* 132:7574–7575.
61. Goose, J. E., and M. S. Sansom. 2013. Reduced lateral mobility of lipids and proteins in crowded membranes. *PLOS Comput. Biol.* 9:e1003033.
62. Pomorski, T., J. C. Holthuis, …, G. van Meer. 2004. Tracking down lipid flippases and their biological functions. *J. Cell Sci.* 117:805–813.
63. Wang, T. Y., and J. R. Silvius. 2001. Cholesterol does not induce segregation of liquid-ordered domains in bilayers modeling the inner leaflet of the plasma membrane. *Biophys. J.* 81:2762–2773.
64. Leventis, R., and J. R. Silvius. 2001. Use of cyclodextrins to monitor transbilayer movement and differential lipid affinities of cholesterol. *Biophys. J.* 81:2257–2267.
65. Chiantia, S., P. Schwille, …, E. London. 2011. Asymmetric GUVs prepared by MβCD-mediated lipid exchange: an FCS study. *Biophys. J.* 100:L1–L3.
66. Hale, J. E., and F. Schroeder. 1982. Asymmetric transbilayer distribution of sterol across plasma membranes determined by fluorescence quenching of dehydroergosterol. *Eur. J. Biochem.* 122:649–661.
67. Mondal, M., B. Mesmin, …, F. R. Maxfield. 2009. Sterols are mainly in the cytoplasmic leaflet of the plasma membrane and the endocytic recycling compartment in CHO cells. *Mol. Biol. Cell.* 20:581–588.
68. Pagler, T. A., M. Wang, …, A. R. Tall. 2011. Deletion of ABCA1 and ABCG1 impairs macrophage migration because of increased Rac1 signaling. *Circ. Res.* 108:194–200.
69. Angelova, M. I., S. Soléau, …, P. Bothorel. 1992. Preparation of giant vesicles by external AC electric fields. kinetics and applications. *Prog. Colloid Polym. Sci.* 89:127–131.
70. Thévenaz, P., U. E. Ruttimann, and M. Unser. 1998. A pyramid approach to subpixel registration based on intensity. *IEEE Trans. Image Process.* 7:27–41.
71. Axelrod, D., D. E. Koppel, …, W. W. Webb. 1976. Mobility measurement by analysis of fluorescence photobleaching recovery kinetics. *Biophys. J.* 16:1055–1069.
72. Kolin, D. L., S. Costantino, and P. W. Wiseman. 2006. Sampling effects, noise, and photobleaching in temporal image correlation spectroscopy. *Biophys. J.* 90:628–639.